

A spectral method for nonlocal diffusion operators on the sphere

Richard Mikaël Slevinsky^{a,*}, Hadrien Montanelli^b, Qiang Du^b

^a*Department of Mathematics, University of Manitoba, Winnipeg, Canada*

^b*Department of Applied Physics and Applied Mathematics, Columbia University, New York, United States*

Abstract

We present algorithms for solving spatially nonlocal diffusion models on the unit sphere with spectral accuracy in space. Our algorithms are based on the diagonalizability of nonlocal diffusion operators in the basis of spherical harmonics, the computation of their eigenvalues to high relative accuracy using quadrature and asymptotic formulas, and a fast spherical harmonic transform. These techniques also lead to an efficient implementation of high-order exponential integrators for time-dependent models. We apply our method to the nonlocal Poisson, Allen–Cahn and Brusselator equations.

Keywords:

nonlocal PDEs on the sphere, nonlocal diffusion operators, spectral methods, fast spherical harmonics, exponential integrators, pattern formation

2010 MSC: 33C55, 42B37, 65D30, 65L05, 65M20, 65M70

1. Introduction

Nonlocal models have been extensively studied in many fields such as materials science, thermodynamics, fluid dynamics, fracture mechanics, biology and image analysis [1, 2, 3, 4, 5, 6]. Many of these models can be conveniently formulated using nonlocal integral operators generalizing the standard differential operators of vector calculus [7, 8]. In this paper, we propose a fast spectral method for computing solutions of nonlocal models of the form

$$u_t = \epsilon^2 \mathcal{L}_\delta u + \mathcal{N}(u), \quad u(t = 0, \mathbf{x}) = u_0(\mathbf{x}), \quad \epsilon > 0, \quad (1)$$

where $u(t, \mathbf{x})$ is a function of time $t \geq 0$ and position \mathbf{x} on the unit sphere $\mathbb{S}^2 \subset \mathbb{R}^3$, \mathcal{N} is a nonlinear operator with constant coefficients (e.g., $\mathcal{N}(u) = u - u^3$), and \mathcal{L}_δ is a nonlocal Laplace–Beltrami operator,

$$\mathcal{L}_\delta u(\mathbf{x}) = \int_{\mathbb{S}^2} \rho_\delta(|\mathbf{x} - \mathbf{y}|) [u(\mathbf{y}) - u(\mathbf{x})] \, d\Omega(\mathbf{y}). \quad (2)$$

In the definition (2) above, $|\mathbf{x} - \mathbf{y}|$ is the Euclidean distance between \mathbf{x} and \mathbf{y} in \mathbb{R}^3 , $d\Omega(\mathbf{y})$ denotes the standard measure on \mathbb{S}^2 and ρ_δ is a suitably defined nonlocal kernel with horizon $0 < \delta \leq 2$, which determines the range of interactions. \mathcal{L}_δ is also called a nonlocal diffusion operator on the sphere. The function u can be real or complex and the equation (1) can be a single equation as well as a system of equations.

There has been substantial work on the numerical approximation of the equation (1) in Euclidean domains [9, 10], including a spectral method for nonlocal diffusion operators defined over a periodic cell in \mathbb{R}^d ($d \leq 3$) [3, 11]. However, no study has been attempted so far to investigate similar discretizations on the sphere. It is of practical interests to study the extension to non-Euclidean geometries with the sphere being a representative example, e.g., for the modelling of anomalous diffusion, pattern formation and image analysis.

*Corresponding author

Email addresses: Richard.Slevinsky@umanitoba.ca (Richard Mikaël Slevinsky), hlm2137@columbia.edu (Hadrien Montanelli), qd2125@columbia.edu (Qiang Du)

URL: <https://home.cc.umanitoba.ca/~slevinrm/> (Richard Mikaël Slevinsky)

For problems defined in spherical geometries there are several methods to discretize the spatial part of the local partial differential equation (PDE) version of the equation (1) with spectral accuracy. The most popular methods include spherical harmonics [12] and the double Fourier sphere (DFS) method [13, 14], recently revisited by Montanelli and Nakatsukasa [15, 16] and Townsend et al. [17]. On the one hand, spherical harmonics are the natural spectral basis for solving local and nonlocal equations on the sphere since they diagonalize both the local and nonlocal Laplace–Beltrami operators, as we will show in Section 2. On the other hand, the DFS method is efficient because it allows one to use two-dimensional fast Fourier transforms (FFTs), which leads to $\mathcal{O}(n^2 \log n)$ complexity per time-step when the spatial part of (1) is discretized at $\mathcal{O}(n^2)$ points.

For spherical harmonics, the picture was quite different before the 2000s. Since a conventional synthesis and analysis of spherical harmonic expansions on tensor-product grids costs $\mathcal{O}(n^3)$, the cost per time-step was not competitive. The picture became more similar from 2006 when Tygert, first with Rokhlin [18] then independently [19, 20], developed asymptotically optimal spherical harmonic transforms with $\mathcal{O}(n^2 \log n)$ run times. The pre-computation was also asymptotically optimal, though this is anticipated only for absurdly high degrees. More recently, Slevinsky proposed two new fast spherical harmonic transforms, first with backward stability, $\mathcal{O}(n^2 \log^2 n)$ run-time and $\mathcal{O}(n^3 \log n)$ pre-computation costs [21], then with $\mathcal{O}(n^2 \log^2 n)$ run-time and $\mathcal{O}(n^{\frac{3}{2}} \log n)$ pre-computation complexities [22]. Equipped with the first fast transform of Slevinsky, we present a spectral method for solving nonlocal diffusion models on the sphere based on eigenvalues and spherical harmonics, which we combine with high-order exponential integrators like ETDRK4 [23] for time-dependent models.

The paper is structured as follows. In Section 2, we prove that the nonlocal Laplace–Beltrami operator on the sphere is diagonalized in the basis of spherical harmonics and derive a closed-form expression for its eigenvalues, which we compute to high relative accuracy in Section 3. We then solve the nonlocal Poisson equation in Section 4 and nonlocal time-dependent equations in Section 5.

2. Eigendata of the nonlocal Laplace–Beltrami operator on the sphere

Let $\mathbf{x} \in \mathbb{S}^2$ be a point on the sphere parameterized by the angles (θ, φ) , where $\theta \in [0, \pi]$ is the colatitude and $\varphi \in [0, 2\pi)$ is the longitude, and let $d\Omega = \sin \theta d\theta d\varphi$ be the measure generated by the solid angle Ω subtended by a spherical cap. The spherical harmonics are given by

$$Y_\ell^m(\mathbf{x}) = Y_\ell^m(\theta, \varphi) = \frac{e^{im\varphi}}{\sqrt{2\pi}} i^{m+|m|} \underbrace{\sqrt{(\ell + \frac{1}{2}) \frac{(\ell - m)!}{(\ell + m)!}}}_{\tilde{P}_\ell^m(\cos \theta)} P_\ell^m(\cos \theta), \quad \ell \geq 0, \quad -\ell \leq m \leq \ell, \quad (3)$$

where the notation \tilde{P}_ℓ^m for the associated Legendre polynomials is used to denote orthonormality for fixed m in the sense of $L^2([-1, 1])$, are eigenfunctions with eigenvalues $-\ell(\ell + 1)$ of the local Laplace–Beltrami operator \mathcal{L}_0 defined by

$$\mathcal{L}_0 u(\theta, \varphi) = u_{\theta\theta} + \frac{\cos \theta}{\sin \theta} u_\theta + \frac{u_{\varphi\varphi}}{\sin^2 \theta}, \quad (4)$$

that is,

$$\mathcal{L}_0 Y_\ell^m(\theta, \varphi) = -\ell(\ell + 1) Y_\ell^m(\theta, \varphi). \quad (5)$$

Spherical harmonics Y_ℓ^m and Legendre polynomials P_ℓ satisfy the addition theorem [12, Eq. (2.27)]

$$P_\ell(\mathbf{x} \cdot \mathbf{y}) = \frac{4\pi}{2\ell + 1} \sum_{m=-\ell}^{+\ell} Y_\ell^m(\mathbf{x}) \overline{Y_\ell^m(\mathbf{y})}, \quad (6)$$

which gives us the integral representation [12, Eq. (2.33)]

$$Y_\ell^m(\mathbf{x}) = \frac{2\ell + 1}{4\pi} \int_{\mathbb{S}^2} P_\ell(\mathbf{x} \cdot \mathbf{y}) Y_\ell^m(\mathbf{y}) d\Omega(\mathbf{y}). \quad (7)$$

Furthermore, for $f \in L^1([-1, 1])$, the Funk–Hecke formula states that [12, Th. 2.22]

$$\int_{\mathbb{S}^2} f(\mathbf{x} \cdot \mathbf{z}) P_\ell(\mathbf{y} \cdot \mathbf{z}) d\Omega(\mathbf{z}) = 2\pi P_\ell(\mathbf{x} \cdot \mathbf{y}) \beta_\ell, \quad \text{where} \quad \beta_\ell = \int_{-1}^1 P_\ell(t) f(t) dt. \quad (8)$$

From the Funk–Hecke formula (8) we obtain the following proposition, which will be useful for our particular choice for the kernel ρ_δ in (2). The proof is given in Appendix A.

Proposition 2.1 (Generalized Funk–Hecke formula). *For a function f with $t \mapsto (1-t)f(t) \in L^1([-1, 1])$, we have*

$$\int_{\mathbb{S}^2} f(\mathbf{x} \cdot \mathbf{z}) [P_\ell(\mathbf{y} \cdot \mathbf{z}) - P_\ell(\mathbf{x} \cdot \mathbf{y})] d\Omega(\mathbf{z}) = 2\pi P_\ell(\mathbf{x} \cdot \mathbf{y}) \gamma_\ell, \quad \gamma_\ell = \int_{-1}^1 [P_\ell(t) - 1] f(t) dt. \quad (9)$$

Let us consider now the nonlocal operator (2). We will set

$$\tilde{\rho}_\delta(\mathbf{x} \cdot \mathbf{y}) = \rho_\delta(|\mathbf{x} - \mathbf{y}|) = \rho_\delta(\sqrt{2(1 - \mathbf{x} \cdot \mathbf{y})}) = \rho_\delta(\sqrt{2(1 - t)}) \quad (10)$$

for brevity, where we used the fact that the Euclidean distance between two points $\mathbf{x}, \mathbf{y} \in \mathbb{S}^2$ is

$$0 \leq |\mathbf{x} - \mathbf{y}| = \sqrt{2(1 - \mathbf{x} \cdot \mathbf{y})} \leq 2. \quad (11)$$

Let us assume that our kernel satisfies $t \mapsto (1-t)\rho_\delta(\sqrt{2(1-t)}) \in L^1([-1, 1])$ so we can use the generalized Funk–Hecke formula (9)—we will come back to this later. If we could find eigenfunctions of the nonlocal operator, then it may be possible to compute eigenvalues as well. For our nonlocal operator, we find

$$\begin{aligned} \mathcal{L}_\delta Y_\ell^m(\mathbf{x}) &= \int_{\mathbb{S}^2} \tilde{\rho}_\delta(\mathbf{x} \cdot \mathbf{z}) [Y_\ell^m(\mathbf{z}) - Y_\ell^m(\mathbf{x})] d\Omega(\mathbf{z}), \\ &= \frac{2\ell+1}{4\pi} \int_{\mathbb{S}^2} \tilde{\rho}_\delta(\mathbf{x} \cdot \mathbf{z}) \int_{\mathbb{S}^2} Y_\ell^m(\mathbf{y}) [P_\ell(\mathbf{y} \cdot \mathbf{z}) - P_\ell(\mathbf{x} \cdot \mathbf{y})] d\Omega(\mathbf{y}) d\Omega(\mathbf{z}), \\ &= \frac{2\ell+1}{4\pi} \int_{\mathbb{S}^2} Y_\ell^m(\mathbf{y}) \int_{\mathbb{S}^2} \tilde{\rho}_\delta(\mathbf{x} \cdot \mathbf{z}) [P_\ell(\mathbf{y} \cdot \mathbf{z}) - P_\ell(\mathbf{x} \cdot \mathbf{y})] d\Omega(\mathbf{z}) d\Omega(\mathbf{y}), \\ &= 2\pi\gamma_\ell \frac{2\ell+1}{4\pi} \int_{\mathbb{S}^2} Y_\ell^m(\mathbf{y}) P_\ell(\mathbf{x} \cdot \mathbf{y}) d\Omega(\mathbf{y}), \\ &= 2\pi\gamma_\ell Y_\ell^m(\mathbf{x}). \end{aligned} \quad (12)$$

Therefore the spherical harmonics Y_ℓ^m are eigenfunctions of the nonlocal Laplace–Beltrami operator (2) with eigenvalues

$$\lambda_\delta(\ell) = 2\pi\gamma_\ell = 2\pi \int_{-1}^1 [P_\ell(t) - 1] \rho_\delta(\sqrt{2(1-t)}) dt. \quad (13)$$

In the following we will focus on the weakly singular kernel

$$\rho_\delta(\sqrt{2(1-t)}) = \frac{(1+\alpha)2^{1+\alpha}}{\pi\delta^{2+2\alpha}(1-t)^{1-\alpha}} \chi_{[0,\delta]}(\sqrt{2(1-t)}), \quad -1 < \alpha < 1, \quad 0 < \delta \leq 2, \quad (14)$$

where $\chi_{[0,\delta]}(\cdot)$ is the indicator function, which results in eigenvalues

$$\lambda_\delta(\ell) = 2\pi \int_d^1 [P_\ell(t) - 1] \rho_\delta(\sqrt{2(1-t)}) dt, \quad d = 1 - \delta^2/2. \quad (15)$$

Note that our kernel satisfies $t \mapsto (1-t)\rho_\delta(\sqrt{2(1-t)}) \in L^1([-1, 1])$, which justifies the use of the generalized Funk–Hecke formula (9) in the derivation of the eigenvalues. The indicator function in (14) is to impose the limit on the range of interactions, and the constants in (14) ensure that for every $\alpha \in (-1, 1)$, $\lambda_\delta \rightarrow \lambda_0$ and $\mathcal{L}_\delta \rightarrow \mathcal{L}_0$ strongly as $\delta \rightarrow 0$ in a suitable operator norm. This statement is proved in Appendix B for an induced operator norm mapping between Sobolev spaces. Note also that this type of kernel is standard for nonlocal models and is the analogue in spherical coordinates of the kernel used for Euclidean domains in [3]. Finally, we expect that the spectral discretization of our nonlocal model (1) on the sphere shares the asymptotic compatibility [24], demonstrated for flat geometries in [11]. Asymptotic compatibility means that the local limit can be preserved at the discrete level and the convergence is uniform with respect to δ as $\delta \rightarrow 0$.

3. Numerical evaluation of the spectrum

A key ingredient of a spectral method is a fast and accurate computation of the spectrum of the underlying operators [25, 26, 27]. In this section we present our numerical method for computing the eigenvalues (15).

3.1. Methodology

We rescale the integral in (15) by

$$t = \frac{1+d}{2} + \frac{1-d}{2}x, \quad (16)$$

such that $t(x) : [-1, 1] \rightarrow [d, 1]$, which yields

$$\lambda_\delta(\ell) = \pi(1-d) \int_{-1}^1 [P_\ell(t(x)) - 1] \rho_\delta(\sqrt{(1-d)(1-x)}) dx. \quad (17)$$

Now, P_ℓ is a degree- ℓ polynomial and

$$\rho_\delta(\sqrt{(1-d)(1-x)}) = \frac{(1+\alpha)2^{1+\alpha}}{\pi\delta^{2+2\alpha}[(\frac{1-d}{2})(1-x)]^{1-\alpha}}. \quad (18)$$

Therefore,

$$\lambda_\delta(\ell) = \frac{(1+\alpha)2^{2+\alpha}}{\delta^{2+2\alpha}} \left(\frac{1-d}{2}\right)^\alpha \int_{-1}^1 [P_\ell(t(x)) - 1] (1-x)^{\alpha-1} dx. \quad (19)$$

This integrand has an algebraic singularity of order $\alpha > -1$ at the right endpoint. To see this, we note that

$$\begin{aligned} P_\ell\left(\frac{1+d}{2} + \frac{1-d}{2}x\right) - 1 &\sim P_\ell(1) - 1 - (1-x) P'_\ell\left(\frac{1+d}{2} + \frac{1-d}{2}x\right) \Big|_{x=1} \\ &= -(1-x) \frac{(1-d)}{2} \frac{\ell(\ell+1)}{2}, \quad \text{as } x \rightarrow 1^-. \end{aligned} \quad (20)$$

Therefore, the final form to integrate is

$$\lambda_\delta(\ell) = \frac{(1+\alpha)2^{2-\alpha}}{\delta^2} \int_{-1}^1 \frac{P_\ell\left[1 - \frac{\delta^2}{2}\left(\frac{1-x}{2}\right)\right] - 1}{1-x} (1-x)^\alpha dx. \quad (21)$$

The hybrid Taylor/RK4 algorithm of Du and Yang [3] requires an ordinary differential equation in terms of a continuously defined eigenvalue with respect to the index ℓ . The difficulty of the spherical eigenvalue formulation is that the oscillations appear due to the degree ℓ of the Legendre polynomials, and derivatives with respect to ℓ unnecessarily complicate the matter. However, the advantage of the spherical eigenvalue formulation is that, compared to the eigenvalue computation on the two-dimensional torus, there are only $n+1$ distinct eigenvalues to calculate for the $(n+1)^2$ spherical harmonics of degree $\leq n$ due to the degeneracy of the spherical harmonics of a particular degree.

The algorithm we propose is to integrate using a modified *Clenshaw–Curtis quadrature* rule. The computational complexity is $O(\ell^2 + \ell \log \ell) = O(\ell^2)$ per eigenvalue $\lambda_\delta(\ell)$, since the integrand requires the numerical evaluation of a degree- ℓ Legendre polynomial at $\ell+1$ points. However, when ℓ is sufficiently large, the integrand evaluation can be replaced by *Szegő's asymptotic formula* [28], which reduces the complexity of pointwise evaluation to $O(1)$ and the overall complexity to $O(\ell + \ell \log \ell) = O(\ell \log \ell)$ per eigenvalue.

Clenshaw–Curtis quadrature. Clenshaw–Curtis quadrature is a quadrature rule [29, 30] whose nodes are the $\ell+1$ Chebyshev–Lobatto points $x_k = \cos(k\pi/\ell)$. Given a continuous weight function $w(x)$ and \mathbb{P}_ℓ , the space of algebraic polynomials of degree at most ℓ , the quadrature weights w_k are determined by

$$\int_{-1}^1 f(x)w(x) dx = \sum_{k=0}^{\ell} w_k f(x_k), \quad \forall f \in \mathbb{P}_\ell. \quad (22)$$

With the modified Chebyshev moments of the weight function

$$\mu_k = \int_{-1}^1 T_k(x)w(x) dx, \quad 0 \leq k \leq \ell, \quad (23)$$

the quadrature weights can be determined via the formula

$$w_j = \frac{1 - \frac{1}{2}(\delta_{0,j} + \delta_{\ell,j})}{\ell} \left[\mu_0 + (-1)^j \mu_\ell + 2 \sum_{k=1}^{\ell-1} \mu_k \cos(\pi j k / \ell) \right], \quad (24)$$

where $\delta_{k,j}$ is the Kronecker delta [31]. Due to this representation, the $O(\ell \log \ell)$ computation of the weights from modified Chebyshev moments is achieved via a diagonally scaled discrete cosine transform.

For the Jacobi weight $w(x) = (1-x)^\alpha(1+x)^\beta$, where $\alpha, \beta > -1$ (which covers our case), the modified Chebyshev moments are known explicitly [32]

$$\mu_\ell^{(\alpha,\beta)} = \int_{-1}^1 T_\ell(x)(1-x)^\alpha(1+x)^\beta dx = 2^{\alpha+\beta+1} B(\alpha+1, \beta+1) {}_3F_2 \left(\begin{matrix} \ell, -\ell, \alpha+1 \\ \frac{1}{2}, \alpha+\beta+2 \end{matrix}; 1 \right), \quad (25)$$

where ${}_3F_2$ is a generalized hypergeometric function [33, §16.2.1] and B is the beta function [33, §5.12.1]. Using Sister Celine's technique [34, §127] or induction [35], a recurrence relation can be derived for the modified moments

$$\mu_0^{(\alpha,\beta)} = 2^{\alpha+\beta+1} B(\alpha+1, \beta+1), \quad \mu_1^{(\alpha,\beta)} = \frac{\beta-\alpha}{\alpha+\beta+2} \mu_0^{(\alpha,\beta)}, \quad (26)$$

$$(\alpha+\beta+\ell+2)\mu_{\ell+1}^{(\alpha,\beta)} + 2(\alpha-\beta)\mu_\ell^{(\alpha,\beta)} + (\alpha+\beta-\ell+2)\mu_{\ell-1}^{(\alpha,\beta)} = 0, \quad \text{for } \ell > 0. \quad (27)$$

Once we have computed the quadrature weights from the modified Chebyshev moments $\mu_\ell^{(\alpha,\beta)}$, all that remains is to evaluate Legendre polynomials at Chebyshev–Lobatto points, which can be done at linear cost per point using the three-term recurrence relation

$$(\ell+1)P_{\ell+1}(t) = (2\ell+1)tP_\ell(t) - \ell P_{\ell-1}(t), \quad (28)$$

or at $O(1)$ cost when ℓ is large enough using Szegő's asymptotic formula.

Szegő's asymptotic formula. Szegő's asymptotic formula [28] for Legendre polynomials is uniformly convergent on $0 \leq \theta < 2(\sqrt{2}-1)\pi$, though special care must be taken at $\theta = 0$. It has been used by Bogaert [36] to develop iteration-free computation of Gauss–Legendre quadrature nodes and weights. The formula is an infinite series in terms of cylindrical Bessel functions

$$P_\ell(\cos \theta) = \sqrt{\frac{\theta}{\sin \theta}} \sum_{\nu=0}^{\infty} \frac{a_\nu(\theta) J_\nu((\ell + \frac{1}{2})\theta)}{(\ell + \frac{1}{2})^\nu}, \quad (29)$$

where the first few coefficient functions $a_\nu(\theta)$ are given by

$$\begin{aligned} a_0(\theta) &= 1, \\ a_1(\theta) &= \frac{1}{8} \frac{\theta \cos \theta - \sin \theta}{\theta \sin \theta}, \\ a_2(\theta) &= \frac{1}{128} \frac{6\theta \sin \theta \cos \theta - 15 \sin^2 \theta + \theta^2(9 - \sin^2 \theta)}{\theta^2 \sin^2 \theta}, \\ a_3(\theta) &= \frac{5}{1024} \frac{((\theta^3 + 21\theta) \sin^2 \theta + 15\theta^3) \cos \theta - ((3\theta^2 + 63) \sin^2 \theta - 27\theta^2) \sin \theta}{\theta^3 \sin^3 \theta}, \end{aligned} \quad (30)$$

and more can be computed by computer algebra systems. In our numerical results, it is clear that even the first four terms provide sufficiently accurate pointwise evaluation for the numerical evaluation of the spectrum to high relative

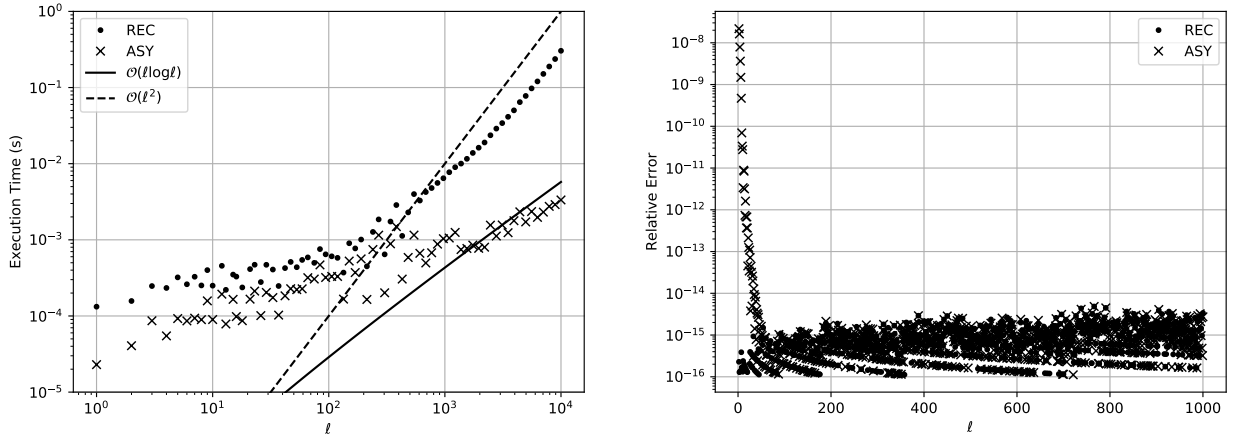


Figure 1: Left: calculation times for the numerical evaluation of $\lambda_1(\ell)$ using the recurrence relation (REC) for the Legendre polynomials and the asymptotics (ASY). Right: approximation to the relative error in the numerical evaluation of $\lambda_1(\ell)$ in IEEE double precision floating-point arithmetic by comparison with numerical results in 256-bit extended precision floating-point arithmetic. In both plots, $\alpha = -0.5$.

accuracy for reasonably low degrees. While it appears that each term in Szegő's asymptotic formula requires the numerical evaluation of an additional cylindrical Bessel function, the recurrence relation,

$$J_{\nu+1}(z) = \frac{2\nu}{z} J_{\nu}(z) - J_{\nu-1}(z), \quad (31)$$

may be employed to reduce the number of evaluations down to two. Normally, the forward recurrence of cylindrical Bessel functions is ill-advised; however, for our purposes only two extra terms are used and their overall contribution is attenuated by the denominator, $(\ell + \frac{1}{2})^{\nu}$. Since $\frac{\pi}{2} < 2(\sqrt{2} - 1)\pi < \pi$, for numerical evaluation on $[\frac{\pi}{2}, \pi]$ we invoke the symmetry relation $P_{\ell}(\cos(\pi - \theta)) = (-1)^{\ell} P_{\ell}(\cos \theta)$.

Stable evaluation for $\theta \approx 0$. Due to the singular nature of the kernel, the numerical evaluation $P_{\ell}(\cos \theta) - 1$ for $\theta \approx 0$ to high relative accuracy is essential. This can be achieved by a local expansion at $\theta = 0$ through the series representation

$$P_{\ell}(\cos \theta) = \sum_{k=0}^{\ell} (-1)^k \binom{\ell}{k} \binom{\ell+k}{k} \sin^{2k} \frac{\theta}{2}. \quad (32)$$

Numerical evaluation of this series allows for the recovery of high relative accuracy for small angles, which is crucial for the accurate evaluation of the weakly singular integral. Furthermore, we may stably divide $P_{\ell}(\cos \theta) - 1$ by $\sin^2 \frac{\theta}{2}$ and the ratio tends to a constant as $\theta \rightarrow 0^+$.

3.2. Numerical experiments

We begin by illustrating calculation times and relative accuracy in the computation of the spectrum (21) by quadrature using the recurrence and asymptotic methods for $\alpha = -0.5$ and $\delta = 1$. For the accuracy, we compute the “exact eigenvalues” $\lambda_1(\ell)$ for $1 \leq \ell \leq 10^3$ using the recurrence in 256-bit extended precision floating-point arithmetic. We show in Figure 1 the calculation times (left) and the relative accuracy (right). As expected the recurrence has quadratic cost while the asymptotics have log-linear cost. In terms of accuracy, the recurrence gives very good accuracy for all ℓ while the asymptotics are accurate only for $\ell > 50$.

In the second experiment we compute the eigenvalues for different values of the strength of the singularity α and the horizon δ . We use the recurrence for $\ell \leq 50$ and the asymptotics for $\ell > 50$. In Figure 2, we plot (minus) the eigenvalues for $\alpha = \pm 0.5$ and $\delta = 0, 0.01, 0.1, 1, \text{ and } 2$. This experiment demonstrates that nonlocal diffusion is

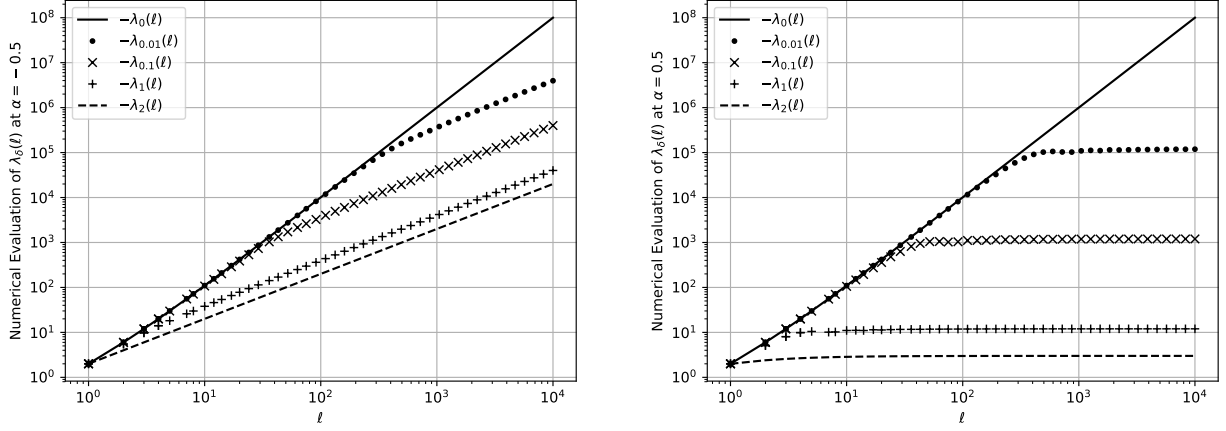


Figure 2: Spectral data $\lambda_\delta(\ell)$ for the nonlocal operator \mathcal{L}_δ with different values of the strength of the singularity α and the horizon δ . Left: for $\alpha = -0.5$. Right: for $\alpha = 0.5$.

asymptotically weaker than its local analogue: the larger α and δ , the weaker. This is reasonable because, for example, the average value of a function over a hemisphere has more inertia than the average value over an infinitesimally small region. Note that for $\alpha = \pm 0.5$ and $\delta = 0$ we recover the eigenvalues $-\ell(\ell + 1)$ of the local operator, while for $\alpha = -0.5$ and $\delta = 2$ we recover the eigenvalues -2ℓ of the nonlocal operator with integration over the entire sphere [12, Eq. (3.74)].

4. Solving the nonlocal Poisson equation

Before solving nonlocal time-dependent models in Section 5, we show how to solve the nonlocal Poisson equation with a mean condition for uniqueness,

$$\begin{aligned} \mathcal{L}_\delta u(\theta, \varphi) &= f(\theta, \varphi), \quad (\theta, \varphi) \in [0, \pi] \times [0, 2\pi], \\ \int_{\mathbb{S}^2} u(\theta, \varphi) \, d\Omega &= \int_{\mathbb{S}^2} f(\theta, \varphi) \, d\Omega. \end{aligned} \quad (33)$$

We discretize colatitude and longitude with a uniform grid with $n + 1$ points in the colatitudinal direction and $2n + 1$ points in the longitudinal direction, and seek a solution $u(\theta, \varphi)$ of degree n of the form

$$u(\theta, \varphi) = \sum_{\ell=0}^n \sum_{m=-\ell}^{+\ell} u_\ell^m Y_\ell^m(\theta, \varphi). \quad (34)$$

The spherical harmonic coefficients u_ℓ^m populate a doubly triangular matrix but for computational purposes, we organize them into the array

$$U = \begin{pmatrix} u_0^0 & u_1^{-1} & u_1^1 & u_2^{-2} & u_2^2 & \dots & u_n^{-n} & u_n^n \\ u_1^0 & u_2^{-1} & u_2^1 & u_3^{-2} & u_3^2 & \dots & 0 & 0 \\ \vdots & \vdots & \vdots & \vdots & \vdots & \ddots & \vdots & \vdots \\ u_{n-2}^0 & u_{n-1}^{-1} & u_{n-1}^1 & u_n^{-2} & u_n^2 & \dots & 0 & 0 \\ u_{n-1}^0 & u_n^{-1} & u_n^1 & 0 & 0 & \dots & 0 & 0 \\ u_n^0 & 0 & 0 & 0 & 0 & \dots & 0 & 0 \end{pmatrix} \in \mathbb{R}^{(n+1) \times (2n+1)}. \quad (35)$$

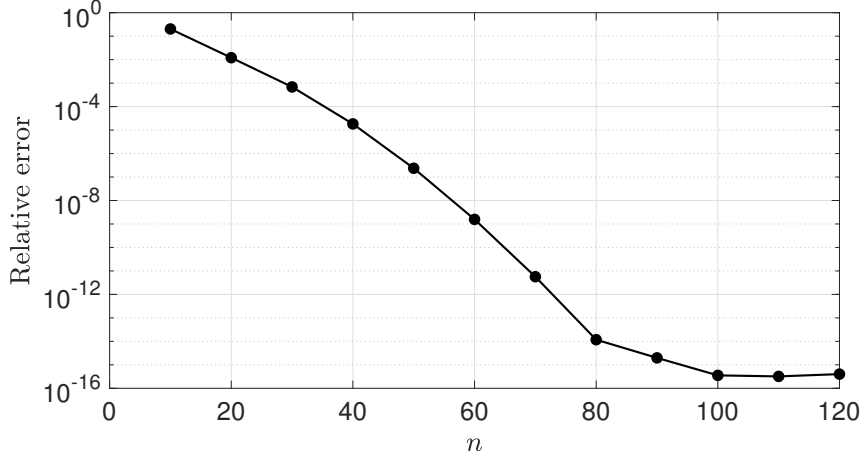


Figure 3: Geometric decay of the 2-norm relative error when solving the nonlocal Poisson equation (33) with right-hand side (40), and parameters $\alpha = -0.5$ and $\delta = 1.5$. One achieves machine accuracy for degrees $n \geq 80$.

The right-hand side f is also expanded in spherical harmonics with coefficients f_ℓ^m , which are stored in an array F .

Note that the mean of u is given by

$$\int_{\mathbb{S}^2} u(\theta, \varphi) d\Omega = u_0^0 Y_0^0 = \frac{u_0^0}{\sqrt{4\pi}}. \quad (36)$$

Therefore u and f have the same mean if and only if $u_0^0 = f_0^0$.

4.1. Nonlocal Laplace–Beltrami matrix

The Laplace–Beltrami operator \mathcal{L}_δ acts diagonally on spherical harmonics so its discretization L_δ is a diagonal singular matrix ($\lambda_\delta(0) = 0$), which we store as an $(n+1) \times (2n+1)$ matrix acting pointwise on the coefficients U , i.e.,

$$L_\delta = \begin{pmatrix} \lambda_\delta(0) & \lambda_\delta(1) & \lambda_\delta(1) & \lambda_\delta(2) & \lambda_\delta(2) & \dots & \lambda_\delta(n) & \lambda_\delta(n) \\ \lambda_\delta(1) & \lambda_\delta(2) & \lambda_\delta(2) & \lambda_\delta(3) & \lambda_\delta(3) & \dots & 0 & 0 \\ \vdots & \vdots & \vdots & \vdots & \vdots & \ddots & \vdots & \vdots \\ \lambda_\delta(n-2) & \lambda_\delta(n-1) & \lambda_\delta(n-1) & \lambda_\delta(n) & \lambda_\delta(n) & \dots & 0 & 0 \\ \lambda_\delta(n-1) & \lambda_\delta(n) & \lambda_\delta(n) & 0 & 0 & \dots & 0 & 0 \\ \lambda_\delta(n) & 0 & 0 & 0 & 0 & \dots & 0 & 0 \end{pmatrix} \in \mathbb{R}^{(n+1) \times (2n+1)}. \quad (37)$$

To make it nonsingular, we impose the mean condition by replacing $\lambda_\delta(0)$ by 1, which gives $u_0^0 = f_0^0$. We then solve

$$L_\delta U = F \quad (38)$$

by simply inverting all the nonzero entries of L_δ pointwise, that is, $U = L_\delta^{-1} F$ with

$$L_\delta^{-1} = \begin{pmatrix} 1 & \lambda_\delta^{-1}(1) & \lambda_\delta^{-1}(1) & \lambda_\delta^{-1}(2) & \lambda_\delta^{-1}(2) & \dots & \lambda_\delta^{-1}(n) & \lambda_\delta^{-1}(n) \\ \lambda_\delta^{-1}(1) & \lambda_\delta^{-1}(2) & \lambda_\delta^{-1}(2) & \lambda_\delta^{-1}(3) & \lambda_\delta^{-1}(3) & \dots & 0 & 0 \\ \vdots & \vdots & \vdots & \vdots & \vdots & \ddots & \vdots & \vdots \\ \lambda_\delta^{-1}(n-2) & \lambda_\delta^{-1}(n-1) & \lambda_\delta^{-1}(n-1) & \lambda_\delta^{-1}(n) & \lambda_\delta^{-1}(n) & \dots & 0 & 0 \\ \lambda_\delta^{-1}(n-1) & \lambda_\delta^{-1}(n) & \lambda_\delta^{-1}(n) & 0 & 0 & \dots & 0 & 0 \\ \lambda_\delta^{-1}(n) & 0 & 0 & 0 & 0 & \dots & 0 & 0 \end{pmatrix}. \quad (39)$$

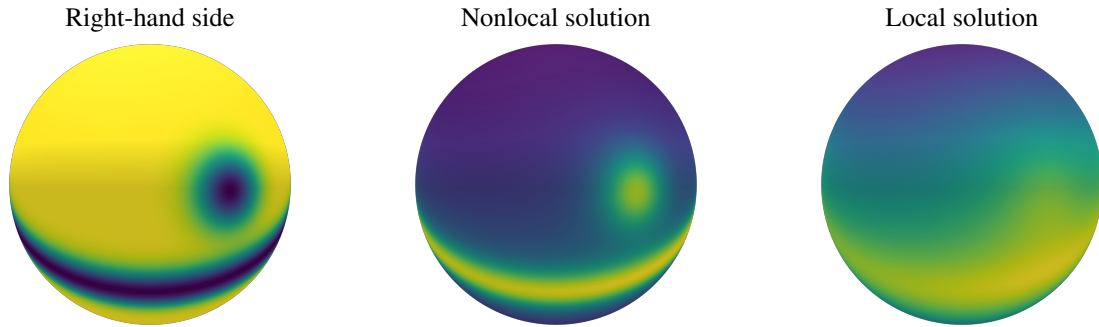


Figure 4: “Death star” right-hand side with nonlocal ($\alpha = 0$, $\delta = 1.5$) and local solutions, which clearly shows that nonlocal diffusion leads to sharper interfaces. The color is scaled to the extrema of the data.

Note that our method could also be applied to the nonlocal Helmholtz equation $\mathcal{L}_\delta u + c^2 u = 0$. Therefore, implicit-explicit time-stepping schemes could also be used to solve time-dependent equations in Section 5.

4.2. Numerical experiments

We solve the nonlocal Poisson equation (33) with a “death star” right-hand side

$$f(x, y, z) = -e^{-30((x-1/4)^2 + (y-\sqrt{11}/4)^2 + (z-1/4)^2)} - e^{-50z^2}, \quad (40)$$

and parameters $\alpha = 0$ and $\delta = 1.5$. We compute the “exact solution” by numerically solving (38) on a very fine grid. We then compute numerical solutions for $n = 10, 20, 30, \dots, 120$ and measure the 2-norm relative error (measured on the coefficients) between numerical and exact solutions. We expect spectral convergence and this is what we observe in Figure 3. The right-hand side together with the local and nonlocal solutions are shown in Figure 4.

5. Solving nonlocal time-dependent equations

For nonlinear nonlocal time-dependent equations of the form (1), we seek solutions of the form

$$u(t, \theta, \varphi) = \sum_{\ell=0}^n \sum_{m=-\ell}^{+\ell} u_\ell^m(t) Y_\ell^m(\theta, \varphi). \quad (41)$$

We obtain a coupled system of nonlinear *ordinary* differential equations,

$$U_t = \epsilon^2 \mathcal{L}_\delta U + N(U), \quad U(0) = U_0, \quad (42)$$

where $U(t)$ represents the $(n+1) \times (2n+1)$ matrix of spherical harmonic coefficients $u_\ell^m(t)$, and the nonlinearity $N(U)$ is evaluated on the grid using a fast spherical harmonic transform.

5.1. Fast spherical harmonic transforms

There are many algorithms available to accelerate synthesis and analysis on the sphere. Our particular choice is the one described by Slevinsky in [21] due to the backward stability that is important for partial differential equations of evolution. We refer the interested reader to [21] for a complete analysis and description of the implementation of the fast spherical harmonic transform.

The steps required by the spherical harmonic connection problem are illustrated in Figure 5. At first, the butterfly algorithm converts higher-order layers of the spherical harmonics into expansions with orders zero and one. Then, these coefficients are rapidly transformed into their Fourier coefficients by the Fast Multipole Method. Total pre-computation requires at best $\mathcal{O}(n^3 \log n)$ flops; and, the asymptotically optimal execution time of $\mathcal{O}(n^2 \log^2 n)$ is rigorously proved via connection to Fourier integral operators, though the asymptotically optimal scaling is anticipated to set it for bandlimits beyond $n \geq \mathcal{O}(20,000)$. Once a spherical harmonic expansion is converted to a bivariate Fourier series, FFTs are able to synthesize function samples at equispaced points-in-angle.

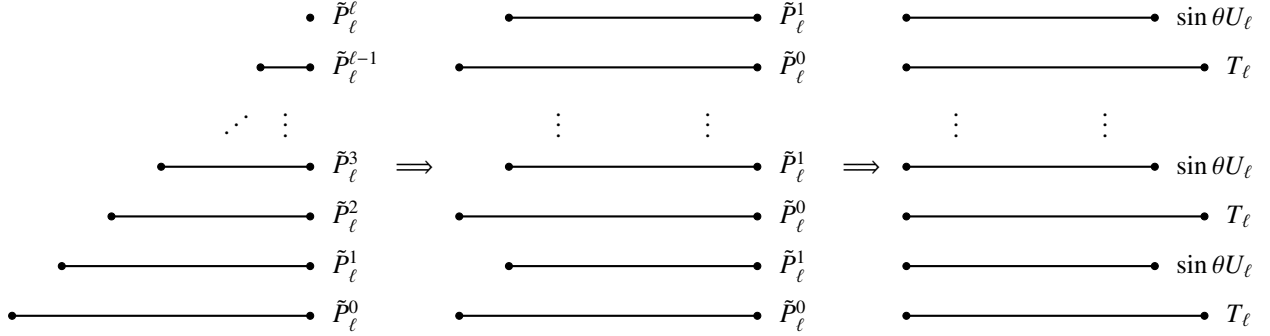


Figure 5: The spherical harmonic transform proceeds in two steps. Firstly, normalized associated Legendre functions are converted to normalized associated Legendre functions of order zero and one. Then, these intermediate expressions are re-expanded in trigonometric form. We use the notation $T_\ell(\cos \theta) = \cos(\ell\theta)$ and $\sin \theta U_\ell(\cos \theta) = \sin((\ell + 1)\theta)$.

5.2. High-order time-stepping with exponential integrators

Time is discretized with a uniform time-step h and the problem is to find the spherical harmonic coefficients U^{k+1} of u at $t_{k+1} = (k + 1)h$ from the coefficients U^k at $t_k = kh$. Since the linear part L_δ in (42) is diagonal, exponential integrators are particularly efficient as the computation of the matrix exponential is equivalent to pointwise exponentiation of the spectrum. For diagonal problems, Montanelli and Bootland recently demonstrated [37] that one of the most effective choices is the ETDRK4 scheme of Cox and Matthews [23]. The formula for this scheme is:

$$\begin{aligned}
 A^k &= e^{\frac{h}{2}L_\delta}U^k + L_\delta^{-1}(e^{hL_\delta} - I)N(U^k), \\
 B^k &= e^{\frac{h}{2}L_\delta}U^k + L_\delta^{-1}(e^{hL_\delta} - I)N(A^k), \\
 C^k &= e^{\frac{h}{2}L_\delta}A^k + L_\delta^{-1}(e^{hL_\delta} - I)[2N(B^k) - N(U^k)], \\
 U^{k+1} &= e^{hL_\delta}U^k + f_1(hL_\delta)N(U^k) + 2f_2(hL_\delta)[N(A^k) + N(B^k)] + f_3(hL_\delta)N(C^k),
 \end{aligned} \tag{43}$$

where the coefficients f_1 , f_2 and f_3 are

$$\begin{aligned}
 f_1(hL_\delta) &= h^{-2}L_\delta^{-3}[-4I - hL_\delta + e^{hL_\delta}(4 - 3hL_\delta + (hL_\delta)^2)], \\
 f_2(hL_\delta) &= h^{-2}L_\delta^{-3}[2I + hL_\delta + e^{hL_\delta}(-2I + hL_\delta)], \\
 f_3(hL_\delta) &= h^{-2}L_\delta^{-3}[-4I - 3hL_\delta - (hL_\delta)^2 + e^{hL_\delta}(4I - hL_\delta)].
 \end{aligned} \tag{44}$$

The stable evaluation of the coefficients may be performed using the contour integral method suggested by Kassam and Trefethen [38]. When working with an eigenfunction expansion, such as the spherical harmonic expansions, it is even more efficient to Taylor expand f_1 , f_2 and f_3 for small argument to recover pointwise evaluation to high relative accuracy. Stability properties of the ETDRK4 scheme have been studied by Du and Zhu in [39]. Note that due to our choice of spherical harmonics for the basis, there is no severe time-step restriction because there are no spurious eigenvalues from discretizing the nonlocal Laplace–Beltrami operator.¹

We note that for equations like (1), one may include linear stabilizing terms to L_δ (that are simultaneously diagonalizable with simple spectrum computation) to help improve the stability. For (1) with special structures, one may also use high-order energy-preserving ETDRK schemes for gradient flows and maximum-principle-preserving ETDRK schemes.

¹In [16], Montanelli and Nakatsukasa discretized the local Laplace–Beltrami operator using the DFS method. The eigenvalues of their Laplace–Beltrami matrix are all real and nonpositive; some of them are spectrally accurate approximations to the eigenvalues $-\ell(\ell + 1)$, but some others, the so-called *outliers*, are of order $O(n^4)$.

5.3. Post-processing data with Cesàro summation

Depending on the relative strength of the diffusive term $\epsilon^2 \mathcal{L}_\delta$ in, e.g., the nonlocal Allen–Cahn equation, the steady-state solution may be discontinuous. This is in contrast to, e.g., the local Allen–Cahn equation that tends to a steady-state consisting of the single constant ± 1 on the entire sphere.

As in the familiar Fourier case (see, e.g., [40, Th. 9.3 of Chap. 2]), the partial sums

$$S_n f(\theta, \varphi) = \sum_{\ell=0}^n \sum_{m=-\ell}^{+\ell} f_\ell^m Y_\ell^m(\theta, \varphi), \quad (45)$$

show the Gibbs phenomenon at points of discontinuity, first described on the sphere by Weyl [41]. The remedy in the Fourier case is to consider instead the arithmetic means of successive partial sums, which do not show the Gibbs phenomenon [40, Th. 3.4 of Chap. 3]. To avoid the Gibbs phenomenon on the sphere, one has to consider Cesàro means of higher order (arithmetic means are Cesàro $(C, 1)$ means). In fact, Dai and Xu show that the (C, κ) means of the spherical harmonic series defined by

$$S_n^\kappa f = \frac{1}{A_n^\kappa} \sum_{\ell=0}^n A_{n-\ell}^\kappa \sum_{m=-\ell}^{+\ell} f_\ell^m Y_\ell^m(\theta, \varphi), \quad A_\ell^\kappa = \binom{\ell + \kappa}{\ell} = \frac{(\kappa + \ell)(\kappa + \ell - 1) \cdots (\kappa + 1)}{\ell!}, \quad (46)$$

completely remove the overshoot of the Gibbs phenomenon when $\kappa \geq 2$ [42, Th. 2.4.3]. Therefore, we post-process our numerical solutions by rescaling the spherical harmonic coefficients using $(C, 2)$ means.²

5.4. Numerical experiments

Allen–Cahn equation. The Allen–Cahn equation, derived by Allen and Cahn in the 1970s, is a reaction-diffusion equation which describes the process of phase separation in iron alloys [44]. It was studied in the ball and on the sphere in [45]. Our nonlocal version on the sphere is

$$u_t = \epsilon^2 \mathcal{L}_\delta u + u - u^3, \quad (47)$$

with nonlocal diffusion $\epsilon^2 \mathcal{L}_\delta u$ and cubic reaction $u - u^3$. The solution u is the order parameter, a correlation function related to the positions of the different components of the alloy. In our experiments, we take $\epsilon = 0.1$, $\alpha = -0.5$, $\delta = 1.0$, and the initial condition

$$u(t = 0, x, y, z) = \cos(10xy). \quad (48)$$

To demonstrate spatial convergence, the 2-norm relative error between the solution obtained with a step size of $h = 2^{-8}$ and varying spherical harmonic degree n versus the solution obtained with $h = 2^{-9}$ and $n = 1023$ is displayed. And for the temporal convergence, the 2-norm relative error between the solution obtained with a spherical harmonic degree $n = 1023$ and varying step sizes h versus the solution obtained with approximately double the degree, $n = 2047$, and half the final step size, $h = 2^{-9}$, is displayed. Note that due to orthonormality of spherical harmonics, the 2-norm relative error at $t = T$ between two approximations expanded in spherical harmonics

$$u_1(t = T, \theta, \varphi) = \sum_{\ell=0}^{\infty} \sum_{m=-\ell}^{+\ell} u_{1,\ell}^m(t = T) Y_\ell^m(\theta, \varphi), \quad u_2(t = T, \theta, \varphi) = \sum_{\ell=0}^{\infty} \sum_{m=-\ell}^{+\ell} u_{2,\ell}^m(t = T) Y_\ell^m(\theta, \varphi), \quad (49)$$

is given by

$$\text{Relative Error at } t = T \approx \frac{\sqrt{\sum_{\ell=0}^{\infty} \sum_{m=-\ell}^{+\ell} |u_{1,\ell}^m(t = T) - u_{2,\ell}^m(t = T)|^2}}{\sqrt{\sum_{\ell=0}^{\infty} \sum_{m=-\ell}^{+\ell} |u_{2,\ell}^m(t = T)|^2}}, \quad (50)$$

²Note that Gelb proposed a method for removing the Gibbs phenomenon for spherical harmonics in [43]. However, her method is limited to the case where the position of the discontinuity is known.

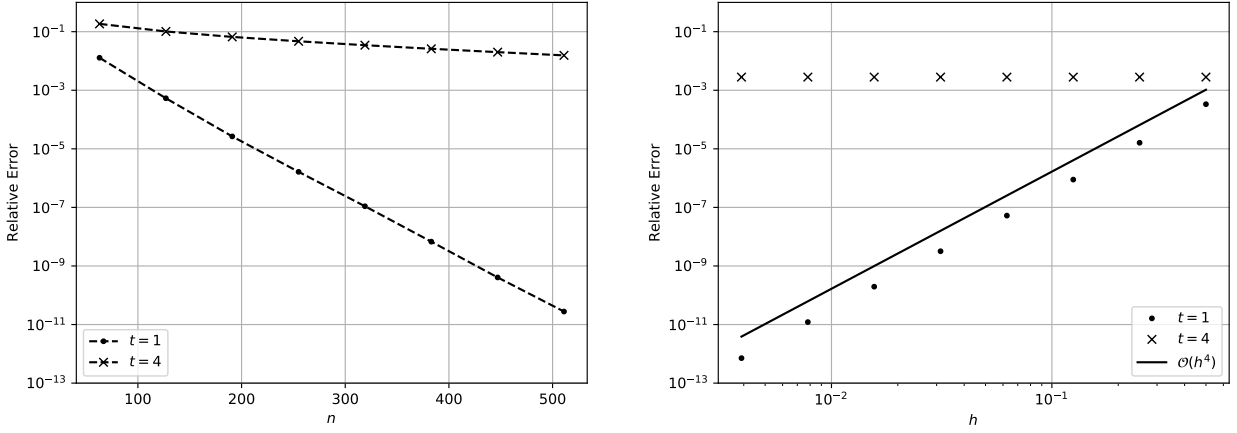


Figure 6: Left: estimates of the spatial error demonstrating spectral convergence. Right: estimates of the temporal error demonstrating fourth-order convergence. In both plots, results show the 2-norm relative error between the computed solution and a computed solution with a finer step size and a larger spherical harmonic degree.

where we have assumed that u_2 is the more accurate approximation to the exact solution.

Figure 6 shows temporal and spatial convergences at times $t = 1$ and $t = 4$. Spectral spatial convergence and fourth-order temporal convergences are demonstrated at time $t = 1$. However, the spectral spatial convergence is significantly attenuated by the time $t = 4$. By extrapolating from the left panel of Figure 6, it is easy to estimate that it would take a spherical harmonic expansion with a degree well beyond current capabilities to even begin to estimate the true fourth-order temporal convergence at $t = 4$. This explains why no temporal convergence is observed at $t = 4$. Furthermore, from the convergence estimates at $t = 4$, Figure 6 invites the possibility that the solution has become discontinuous in finite time.

The qualitative differences in the solutions of the local and nonlocal Allen–Cahn equations are most deftly observed by comparing simulations with random initial conditions. Therefore, in Figure 7, a random initial condition and the solution at a geometrical time progression depict the fundamentally different qualitative behaviors of the local and nonlocal equations. In Figure 7, the same ϵ , α , and δ are used, and the time steps are $h = 10^{-1}$ and the maximal spherical harmonic degree is $n = 511$. We also show in Figure 8 the evolution of the nonlocal Ginzburg–Landau free energy

$$\mathcal{E}(u) = \int_{\mathbb{S}^2} \left[-\frac{\epsilon^2}{2} u \mathcal{L}_\delta u + \frac{1}{4} (u^2 - 1)^2 \right] d\Omega. \quad (51)$$

Brusselator equations. The dynamics of spot patterns in the Brusselator model for reaction-diffusion systems on the sphere was studied by Trinh and Ward in [46]. A nonlocal version of the Brusselator equations is defined by the coupled system

$$\begin{cases} u_t = \epsilon^2 \mathcal{L}_\delta u + \epsilon^2 E - u + f u^2 v, \\ \tau v_t = \mathcal{L}_\delta v + \epsilon^{-2} (u - u^2 v), \end{cases} \quad (52)$$

for some constants $E > 0$, $\epsilon > 0$, $\tau > 0$, and $0 < f < 1$. By perturbing the steady-state equilibria

$$u_e = \frac{\epsilon^2 E}{1 - f} = v_e^{-1}, \quad (53)$$

by as little as a 1% fluctuation, the emergence of localized spot patterns is observed [46]. In Figure 9, we consider a similar random initial condition with the same parameter values $E = 4$, $\epsilon = 0.075$, $\tau = 7.8125$, and $f = 0.8$ but also

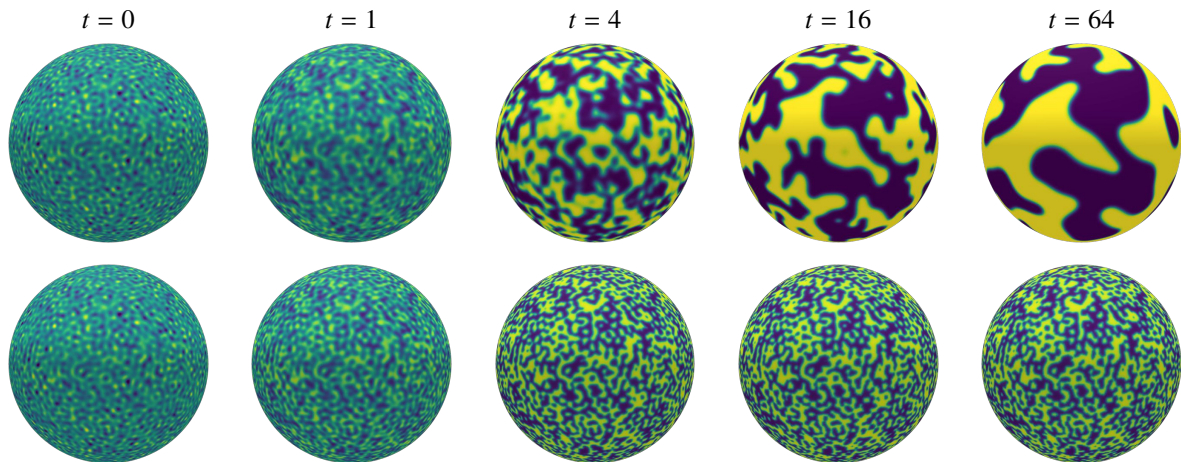


Figure 7: Time evolution of the local (top) and nonlocal (bottom) Allen–Cahn equation starting with a random initial condition provided by a spherical harmonic expansion with the first 128^2 standard normally distributed numbers seeded by `srnd(0)` and scaled by 128^{-1} used to populate all coefficients of degree ≤ 127 .

consider the reaction with a nonlocal diffusion. In contrast to previous figures, the color is now scaled to the extrema of the solutions u and v , with the extrema shown below each plot. Whereas we replicate a similar spot pattern for the localized diffusion, when the nonlocal diffusion operator with $\alpha = 0$, $\delta = 1$, $n = 399$, and $h = 10^{-1}$, the solution is speckled.

6. Discussion

We have presented algorithms for solving nonlocal diffusion models on the sphere with spectral accuracy in space and high-order accuracy in time. These are based on the diagonalization of the nonlocal Laplace–Beltrami operator, the high-accuracy computation of their eigenvalues, a fast spherical harmonic transform and exponential integrators. We have applied our method to the nonlocal Allen–Cahn and Brusselator equations. Notwithstanding the potential convergence to discontinuous equilibria accompanied by the Gibbs phenomenon, we are able to remove the non-physical oscillations by the use of Cesàro means.

Our JULIA codes are available online at *GitHub* (`FastTransforms.jl` and `SpectralTimeStepping.jl` packages). A MATLAB version, based on Chebfun [47] and its recent extensions to periodic problems [48] and the sphere [16, 17] and `mex-ing` in the fast spherical harmonic transform from JULIA, is available upon request.

There are many ways to continue the analysis of nonlocal diffusion operators on the sphere. Nonlocal diffusion operators introduce new qualitative behaviors in contrast to classical PDEs of evolution and their steady-states. Indeed, nonlocal interactions are ubiquitous in nature and they are also generic features of model reduction [10].

Our first particular choice of a nonlocal diffusion operator (2) is motivated by an expedited numerical analysis of the spectrum. Another choice for a nonlocal operator is the fractional Laplacian,³ and yet another reasonable modification is to use geodesic distance in place of Euclidean distance. In [49], a general approach is used for singular integral equations that could well be adapted to more general kernels $\rho_\delta(\mathbf{x}, \mathbf{y})$ in the present setting. While beyond the scope of this report, one may argue that the nonlocal diffusion operator (2) provides many of the qualitative behaviors that one might expect, has a natural integral definition that may be related to measurable physical quantities, and also has a few parameters that may be useful for modelling purposes. Furthermore, the Euclidean and geodesic distances are isomorphic and a function of either one may be rapidly expanded as a series of functions of the other.

³It can be shown that the fractional Laplacian corresponds to our nonlocal operator with particular choices of the parameters α and δ for which the numerical integration may be performed exactly.

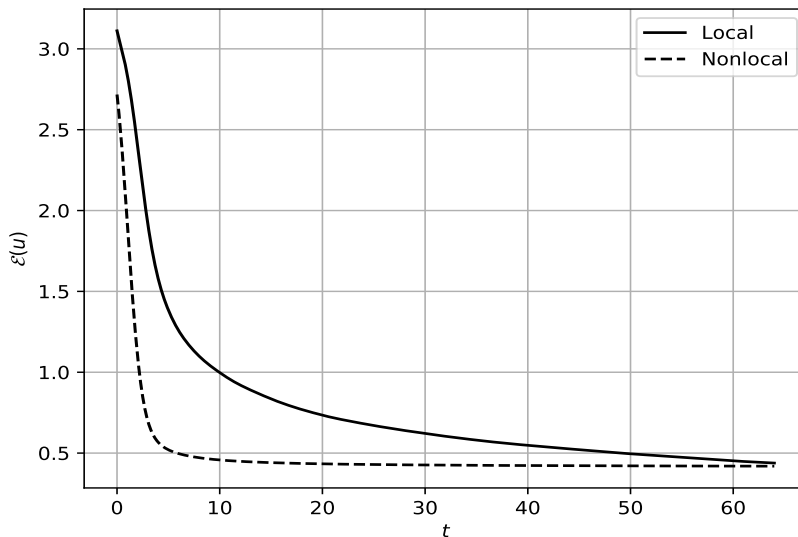


Figure 8: Evolution of the Ginzburg–Landau free energies of the local and nonlocal solutions depicted in Figure 7. Both free energies are decreasing functions of time, confirming that the spatial and temporal accuracies are sufficient to exhibit correct qualitative behavior. It appears that the nonlocal free energy may be positively bounded below, while the local free energy appears to continue to decrease.

While the steady-state of the nonlocal Allen–Cahn equation is known to be possibly discontinuous [11], a potential topic for the analysis of nonlocal operators is whether discontinuities are attained in finite or infinite time. The spatial convergence of spectral methods, such as ours, assimilate the regularity of the solution: for analytic or entire solutions, this property makes them extremely competitive, structured linear algebra permitting; for discontinuous solutions, Cesàro means remove the Gibbs phenomenon, but it is not clear that a spectral method may perform any better or worse than a finite difference/element/volume method. An advantage of the spherical harmonic basis is the trivial computation of the spectrum of the nonlocal operator. If another spatial discretization were chosen, it is possible for this to become the bottleneck in the simulation of the evolution of the dynamical system. Another advantage is that we expect spectral accuracy *arbitrarily close to* the discontinuous steady-state if the initial condition is sufficiently smooth.

Other extensions include the design of similar algorithms for higher-order diffusion or gradient-type operators, and the numerical solution of nonlocal PDEs on spheroids and other manifolds. Nonlocal phase-field crystal models on the sphere could also be an exciting application.

Acknowledgments

We thank the members of the CM3 group (Ran Gu, Hwi Lee, Qi Sun and Yunzhe Tao) at Columbia University for fruitful discussions. We thank Feng Dai for an enlightening discussion on Cesàro means. We also thank Nick Trefethen for introducing us to Ignace Bogaert, who so effectively demonstrates the utility of Szegő’s asymptotic formula for iteration-free Gauss–Legendre quadrature. Finally, we would like to express our gratitude to the reviewers (Alex Townsend and the anonymous one) for their constructive reports. Their comments and suggestions helped us to significantly improve the quality of the manuscript. This research is supported in part by NSERC RGPIN-2017-05514, NSF DMS-1719699, AFOSR MURI center for material failure prediction through peridynamics, and the ARO MURI Grant W911NF-15-1-0562.

- [1] P. W. Bates, A. Chmaj, An integrodifferential model for phase transitions: stationary solutions in higher space dimensions, *J. Stat. Phys.* 95 (1999) 1119–1139.

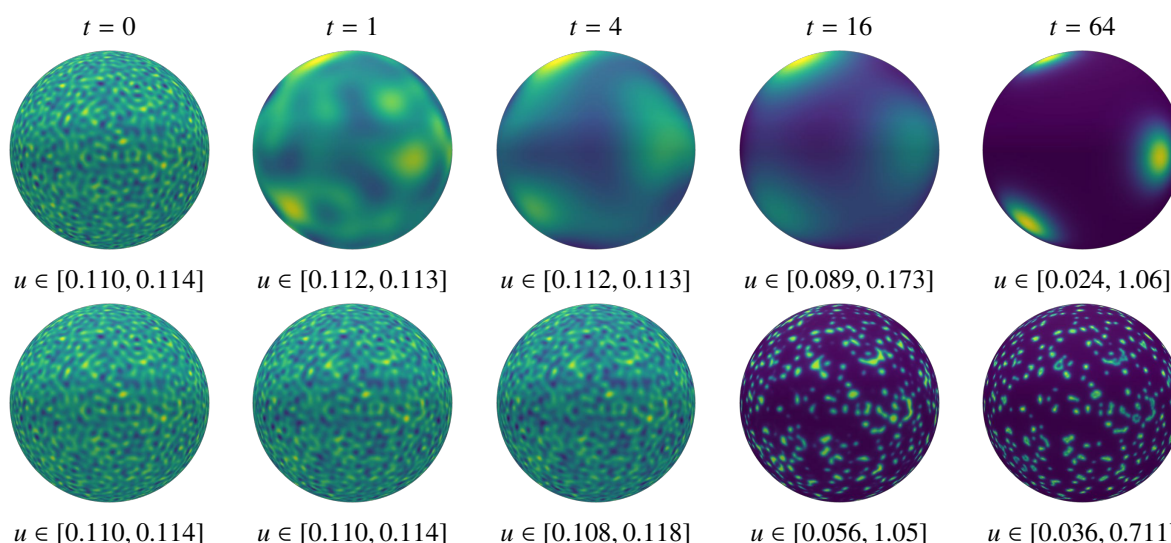


Figure 9: Time evolution of the local (top) and nonlocal (bottom) Brusselator equations with the same parameter values as in [46] and a similar random initial perturbation of the steady-states provided by a spherical harmonic expansion with the first 2×100^2 standard normally distributed numbers seeded by `srand(0)` and scaled by $(\pi \times 100 \times 100)^{-1}$ used to populate all coefficients of degree ≤ 99 , half for each initial condition.

- [2] F. Bobaru, M. Duangpanya, The peridynamic formulation for transient heat conduction, *Int. J. Heat Mass Tranf.* 53 (2010) 4047–4059.
- [3] Q. Du, J. Yang, Fast and accurate implementation of Fourier spectral approximations of nonlocal diffusion operators and its applications, *J. Comput. Phys* 332 (2017) 118–134.
- [4] G. Gilboa, S. Osher, Nonlocal operators with applications to image processing, *Multiscale Model. Simul.* 7 (3) (2008) 1005–1028.
- [5] C.-Y. Kao, Y. Lou, W. Shen, Random dispersal vs. non-local dispersal, *Discrete Contin. Dyn. Syst.* 26 (2) (2010) 551–596.
- [6] S. A. Silling, Reformulation of elasticity theory for discontinuities and long-range forces, *J. Mech. Phys. Solids* 48 (2000) 175–209.
- [7] Q. Du, M. Gunzburger, R. B. Lehoucq, K. Zhou, Analysis and approximation of nonlocal diffusion problems with volume constraints, *SIAM Rev.* 54 (2012) 667–696.
- [8] Q. Du, M. Gunzburger, R. B. Lehoucq, K. Zhou, A nonlocal vector calculus, nonlocal volume-constrained problems, and nonlocal balance laws, *Math. Models Methods Appl. Sci.* 23 (2013) 493–540.
- [9] Q. Du, Local limits and asymptotically compatible discretizations, in: *Handbook of peridynamic modeling*, Adv. Appl. Math., CRC Press, Boca Raton, 2017, pp. 87–108.
- [10] Q. Du, *Nonlocal modeling, analysis and computation*, NSF-CBMS Monograph, SIAM, Philadelphia, 2018.
- [11] Q. Du, J. Yang, Asymptotically compatible Fourier spectral approximations of nonlocal Allen–Cahn equations, *SIAM J. Numer. Anal.* 54 (2016) 1899–1919.
- [12] K. Atkinson, W. Han, *Spherical Harmonics and Approximations on the Unit Sphere: An Introduction*, Springer, Berlin, 2012.
- [13] P. E. Merilees, The pseudospectral approximation applied to the shallow water equations on a sphere, *Atmosphere* 11 (1973) 13–20.
- [14] S. A. Orszag, Fourier series on spheres, *Mon. Wea. Rev.* 102 (1974) 56–75.
- [15] H. Montanelli, Numerical algorithms for differential equations with periodicity, Ph.D. thesis, University of Oxford (2017).
- [16] H. Montanelli, Y. Nakatsukasa, Fourth-order time-stepping for stiff PDEs on the sphere, arXiv:1701.06030, 2017.
- [17] A. Townsend, H. Wilber, G. B. Wright, Computing with functions in spherical and polar geometries, I. The sphere, *SIAM J. Sci. Comput.* 38 (2016) C403–C425.
- [18] V. Rokhlin, M. Tygert, Fast algorithms for spherical harmonic expansions, *SIAM J. Sci. Comput.* 27 (2006) 1903–1928.
- [19] M. Tygert, Fast algorithms for spherical harmonic expansions, II, *J. Comput. Phys.* 227 (2008) 4260–4279.
- [20] M. Tygert, Fast algorithms for spherical harmonic expansions, III, *J. Comput. Phys.* 229 (2010) 6181–6192.
- [21] R. M. Slevinsky, Fast and backward stable transforms between spherical harmonic expansions and bivariate Fourier series, *Appl. Comput. Harmon. Anal.*
- [22] R. M. Slevinsky, Conquering the pre-computation in two-dimensional harmonic polynomial transforms, arXiv:1711.07866 (2017).
- [23] S. M. Cox, P. C. Matthews, Exponential time differencing for stiff systems, *J. Comput. Phys.* 176 (2002) 430–455.
- [24] X. Tian, Q. Du, Analysis and comparison of different approximations to nonlocal diffusion and linear peridynamic equations, *SIAM J. Numer. Anal.* 51 (6) (2013) 3458–3482.
- [25] L. N. Trefethen, *Spectral Methods in MATLAB*, SIAM, Philadelphia, 2000.
- [26] C. Canuto, M. Y. Hussaini, A. Quarteroni, T. A. Zang, *Spectral Methods: Evolution to Complex Geometries and Applications to Fluid Dynamics*, Springer, Berlin, 2007.
- [27] J. Shen, T. Tang, L.-L. Wang, *Spectral Methods: Algorithms, Analysis and Applications*, Springer, Berlin, 2011.
- [28] G. Szegő, Über einige asymptotische entwicklungen der Legendreschen funktionen, *Proc. Lond. Math. Soc.* 50 (1934) 427–450.
- [29] A. Sommariva, Fast construction of Fejér and Clenshaw–Curtis rules for general weight functions, *Comp. Math. Appl.* 65 (2013) 682–693.

- [30] J. Waldvogel, Fast construction of the Fejér and Clenshaw–Curtis quadrature rules, *BIT Numer. Math.* 46 (2006) 195–202.
- [31] M. Abramowitz, I. A. Stegun, *Handbook of Mathematical Functions with Formulas, Graphs, and Mathematical Tables*, Dover Publications, New York, 1965.
- [32] R. Piessens, Modified Clenshaw–Curtis integration and applications to numerical computation of integral transforms, in: P. Keast, G. Fairweather (Eds.), *Numerical Integration: Recent Developments, Software and Applications*, Springer Netherlands, Dordrecht, 1987, pp. 35–51.
- [33] F. W. J. Olver, D. W. Lozier, R. F. Boisvert, C. W. Clark, *NIST Handbook of Mathematical Functions*, Cambridge University Press, Cambridge, 2010.
- [34] E. Rainville, *Special Functions*, MacMillan, New York, 1960.
- [35] S. Xiang, G. He, H. Wang, On fast and stable implementation of Clenshaw–Curtis and Fejér-type quadrature rules, *Abst. Appl. Anal.* 2014.
- [36] I. Bogaert, Iteration-free computation of Gauss–Legendre quadrature nodes and weights, *SIAM J. Sci. Comput.* 36 (2014) A1008–A1026.
- [37] H. Montanelli, N. Bootland, Solving periodic semilinear stiff PDEs in 1D, 2D and 3D with exponential integrators, arXiv:1604.08900, 2016.
- [38] A.-K. Kassam, L. N. Trefethen, Fourth-order time-stepping for stiff PDEs, *SIAM J. Sci. Comput.* 26 (2005) 1214–1233.
- [39] Q. Du, W. Zhu, Analysis and applications of the exponential time differencing schemes and their contour integral modifications, *BIT Numer. Math.* 45 (2005) 307–328.
- [40] A. Zygmund, *Trigonometric Series*, Cambridge University Press, Cambridge, 1959.
- [41] H. Weyl, Die Gibbssche Erscheinung in der Theorie der Kugelfunktionen, *Rend. Circ. Matem. Palermo* 29 (1910) 308–323.
- [42] F. Dai, Y. Xu, *Approximation Theory and Harmonic Analysis on Spheres and Balls*, Springer, New York, 2013.
- [43] A. Gelb, The resolution of the Gibbs phenomenon for spherical harmonics, *Math. Comp.* 66 (1997) 699–717.
- [44] S. M. Allen, J. W. Cahn, A microscopic theory for antiphase boundary motion and its application to antiphase domain coarsening, *Acta Metall.* 27 (1979) 1085–1095.
- [45] Y. Du, The heterogeneous Allen–Cahn equation in a ball: Solutions with layers and spikes, *J. Differential Equations* 244 (2008) 117–169.
- [46] P. H. Trinh, M. J. Ward, The dynamics of localized spot patterns for reaction–diffusion systems on the sphere, *Nonlinearity* 29 (2016) 766–806.
- [47] T. A. Driscoll, N. Hale, L. N. Trefethen (Eds.), *Chebfun Guide*, Pafnuty Publications, Oxford, 2014; see also www.chebfun.org.
- [48] G. B. Wright, M. Javed, H. Montanelli, L. N. Trefethen, Extension of Chebfun to periodic functions, *SIAM J. Sci. Comput.* 37 (2015) C554–C573.
- [49] R. M. Slevinsky, S. Olver, A fast and well-conditioned spectral method for singular integral equations, *J. Comp. Phys.* 332 (2017) 290–315.

A. Proof of the generalized Funk–Hecke formula

Lemma A.1. *Provided $t \mapsto (1 - t)f(t) \in L^1([-1, 1])$,*

$$\left| \int_{\mathbb{S}^2} f(\mathbf{x} \cdot \mathbf{z}) [P_\ell(\mathbf{y} \cdot \mathbf{z}) - P_\ell(\mathbf{x} \cdot \mathbf{y})] d\Omega(\mathbf{z}) \right| < +\infty. \quad (\text{A.1})$$

Proof. Without loss of generality, we assume that $\mathbf{x} = (0, 0, 1)^\top$ is located at the North pole. If it were not, we could introduce an orthogonal rotation of coordinates to make it so. Then, let

$$\mathbf{y} = (y_1, y_2, y_3)^\top \quad \text{and} \quad \mathbf{z} = (\sin \theta \cos \varphi, \sin \theta \sin \varphi, \cos \theta)^\top, \quad (\text{A.2})$$

be the other points on the sphere. We may write

$$\begin{aligned} & \int_{\mathbb{S}^2} f(\mathbf{x} \cdot \mathbf{z}) [P_\ell(\mathbf{y} \cdot \mathbf{z}) - P_\ell(\mathbf{x} \cdot \mathbf{y})] d\Omega(\mathbf{z}), \\ &= \int_{\mathbb{S}^2} (1 - \mathbf{x} \cdot \mathbf{z}) f(\mathbf{x} \cdot \mathbf{z}) \frac{\mathbf{y} \cdot \mathbf{z} - \mathbf{x} \cdot \mathbf{y}}{1 - \mathbf{x} \cdot \mathbf{z}} \frac{P_\ell(\mathbf{y} \cdot \mathbf{z}) - P_\ell(\mathbf{x} \cdot \mathbf{y})}{\mathbf{y} \cdot \mathbf{z} - \mathbf{x} \cdot \mathbf{y}} d\Omega(\mathbf{z}), \end{aligned} \quad (\text{A.3})$$

provided we characterize the singularities that are introduced. The last term is bounded, for

$$\lim_{\mathbf{y} \cdot \mathbf{z} \rightarrow \mathbf{x} \cdot \mathbf{y}} \frac{P_\ell(\mathbf{y} \cdot \mathbf{z}) - P_\ell(\mathbf{x} \cdot \mathbf{y})}{\mathbf{y} \cdot \mathbf{z} - \mathbf{x} \cdot \mathbf{y}} = P'_\ell(\mathbf{x} \cdot \mathbf{y}). \quad (\text{A.4})$$

Since it is a rational function with a single removable singularity, it has a finite spherical harmonic series,

$$\frac{P_\ell(\mathbf{y} \cdot \mathbf{z}) - P_\ell(\mathbf{x} \cdot \mathbf{y})}{\mathbf{y} \cdot \mathbf{z} - \mathbf{x} \cdot \mathbf{y}} = \sum_{\lambda=0}^{\ell-1} \sum_{m=-\lambda}^{+\lambda} u_\lambda^m(\mathbf{x}, \mathbf{y}) Y_\lambda^m(\mathbf{z}), \quad (\text{A.5})$$

where the coefficients are functions of \mathbf{x} and \mathbf{y} . In terms of the spherical coordinates, the second term is

$$\frac{\mathbf{y} \cdot \mathbf{z} - \mathbf{x} \cdot \mathbf{y}}{1 - \mathbf{x} \cdot \mathbf{z}} = \frac{(y_1 \cos \varphi + y_2 \sin \varphi) \sin \theta + y_3 (\cos \theta - 1)}{1 - \cos \theta}. \quad (\text{A.6})$$

Then the integral is

$$\begin{aligned}
& \int_{\mathbb{S}^2} f(\mathbf{x} \cdot \mathbf{z}) [P_\ell(\mathbf{y} \cdot \mathbf{z}) - P_\ell(\mathbf{x} \cdot \mathbf{y})] d\Omega(\mathbf{z}), \\
&= \lim_{\varepsilon \rightarrow 0^+} \int_\varepsilon^\pi (1 - \cos \theta) f(\cos \theta) \sin \theta d\theta \\
&\quad \times \int_0^{2\pi} \frac{(y_1 \cos \varphi + y_2 \sin \varphi) \sin \theta + y_3(\cos \theta - 1)}{1 - \cos \theta} \frac{P_\ell(\mathbf{y} \cdot \mathbf{z}) - P_\ell(\mathbf{x} \cdot \mathbf{y})}{\mathbf{y} \cdot \mathbf{z} - \mathbf{x} \cdot \mathbf{y}} d\varphi, \\
&= \sum_{\lambda=0}^{\ell-1} \sum_{m=-\lambda}^{+\lambda} u_\lambda^m(\mathbf{x}, \mathbf{y}) \lim_{\varepsilon \rightarrow 0^+} \int_\varepsilon^\pi (1 - \cos \theta) f(\cos \theta) \sin \theta d\theta \\
&\quad \times \int_0^{2\pi} \frac{(y_1 \cos \varphi + y_2 \sin \varphi) \sin \theta + y_3(\cos \theta - 1)}{1 - \cos \theta} Y_\lambda^m(\theta, \varphi) d\varphi.
\end{aligned} \tag{A.7}$$

There are two cases to consider. On the one hand, if $m = 0$, then $Y_\lambda^0(\theta, \varphi)$ is independent of φ , and

$$\begin{aligned}
& \int_0^{2\pi} \frac{(y_1 \cos \varphi + y_2 \sin \varphi) \sin \theta + y_3(\cos \theta - 1)}{1 - \cos \theta} Y_\lambda^0(\theta, \varphi) d\varphi, \\
&= \int_0^{2\pi} \frac{y_3(\cos \theta - 1)}{1 - \cos \theta} Y_\lambda^0(\theta, \varphi) d\varphi = -2\pi y_3 Y_\lambda^0(\theta, \varphi).
\end{aligned} \tag{A.8}$$

On the other hand, if $|m| > 0$, then the spherical harmonics contain at least a power of $\sin \theta$ such that

$$\frac{\sin \theta Y_\lambda^m(\theta, \varphi)}{1 - \cos \theta} \tag{A.9}$$

has a removable singularity as $\theta \rightarrow 0^+$, proving that the integral in Equation (A.1) is bounded. \square

Proof of Proposition 2.1. First, let us note that by Lemma A.1 the left-hand side of (9) is bounded. Let us now focus on the right-hand side of (9) and consider the sequence f_k of non-negative and *integrable* functions defined by⁴

$$0 \leq f_k(t) = \begin{cases} 0, & t \in \{|f(t)| > k\} \cap \{t > 1 - 1/k\}, \\ f(t), & \text{otherwise.} \end{cases} \tag{A.10}$$

The generalized Funk–Hecke formula is clearly true for any f_k as the Funk–Hecke formula is applicable in both instances with P_ℓ and $P_0 = 1$, respectively. For any $\varepsilon > 0$, let us write

$$\gamma_\ell = \int_{-1}^1 [P_\ell(t) - 1] f(t) dt = \int_{-1}^{1-\varepsilon} [P_\ell(t) - 1] f(t) dt + \int_{1-\varepsilon}^1 [P_\ell(t) - 1] f(t) dt. \tag{A.11}$$

Then there is a $K = K(\varepsilon) > \varepsilon^{-1}$ such that for any $k \geq K$, f and f_k coincide on $[-1, 1 - \varepsilon]$. Therefore

$$\gamma_\ell = \int_{-1}^{1-\varepsilon} [P_\ell(t) - 1] f_k(t) dt + \int_{1-\varepsilon}^1 [P_\ell(t) - 1] f(t) dt, \tag{A.12}$$

for some $k \geq K$. By adding and subtracting $\int_{1-\varepsilon}^1 [P_\ell(t) - 1] f_k(t) dt$ to (A.12) we obtain

$$\gamma_\ell = \int_{-1}^1 [P_\ell(t) - 1] f_k(t) dt + \int_{1-\varepsilon}^1 [P_\ell(t) - 1] f(t) dt - \int_{1-\varepsilon}^1 [P_\ell(t) - 1] f_k(t) dt. \tag{A.13}$$

⁴This does not limit the proof to non-negative functions for we may split f into $f^+ = \max\{f, 0\}$ and $f^- = \min\{f, 0\}$. However, it does simplify the argument.

The first term on the right-hand side of (A.13), multiplied by $2\pi P_\ell(\mathbf{x} \cdot \mathbf{y})$, can be rewritten as

$$2\pi P_\ell(\mathbf{x} \cdot \mathbf{y}) \int_{-1}^1 [P_\ell(t) - 1] f_k(t) dt = \int_{\mathbb{S}^2} f_k(\mathbf{x} \cdot \mathbf{z}) [P_\ell(\mathbf{y} \cdot \mathbf{z}) - P_\ell(\mathbf{x} \cdot \mathbf{y})] d\Omega(\mathbf{z}), \quad (\text{A.14})$$

using the generalized Funk–Hecke formula for f_k . Let us denote by $C_\varepsilon(\mathbf{x}) = \{\mathbf{z} \in \mathbb{S}^2 : 1 - \varepsilon \leq \mathbf{z} \cdot \mathbf{x} \leq 1\}$ the region on the sphere for which $f_k \neq f$. We can rewrite (A.14) as

$$\begin{aligned} & 2\pi P_\ell(\mathbf{x} \cdot \mathbf{y}) \int_{-1}^1 [P_\ell(t) - 1] f_k(t) dt, \\ &= \int_{\mathbb{S}^2 \setminus C_\varepsilon(\mathbf{x})} f(\mathbf{x} \cdot \mathbf{z}) [P_\ell(\mathbf{y} \cdot \mathbf{z}) - P_\ell(\mathbf{x} \cdot \mathbf{y})] d\Omega(\mathbf{z}), \\ &= \int_{\mathbb{S}^2} f(\mathbf{x} \cdot \mathbf{z}) [P_\ell(\mathbf{y} \cdot \mathbf{z}) - P_\ell(\mathbf{x} \cdot \mathbf{y})] d\Omega(\mathbf{z}) - \int_{C_\varepsilon(\mathbf{x})} f(\mathbf{x} \cdot \mathbf{z}) [P_\ell(\mathbf{y} \cdot \mathbf{z}) - P_\ell(\mathbf{x} \cdot \mathbf{y})] d\Omega(\mathbf{z}). \end{aligned} \quad (\text{A.15})$$

Combining (A.13), multiplied by $2\pi P_\ell(\mathbf{x} \cdot \mathbf{y})$, with (A.15) yields

$$\begin{aligned} 2\pi P_\ell(\mathbf{x} \cdot \mathbf{y}) \gamma_\ell &= \int_{\mathbb{S}^2} f(\mathbf{x} \cdot \mathbf{z}) [P_\ell(\mathbf{y} \cdot \mathbf{z}) - P_\ell(\mathbf{x} \cdot \mathbf{y})] d\Omega(\mathbf{z}) - \int_{C_\varepsilon(\mathbf{x})} f(\mathbf{x} \cdot \mathbf{z}) [P_\ell(\mathbf{y} \cdot \mathbf{z}) - P_\ell(\mathbf{x} \cdot \mathbf{y})] d\Omega(\mathbf{z}) \\ &\quad + 2\pi P_\ell(\mathbf{x} \cdot \mathbf{y}) \left[\int_{1-\varepsilon}^1 [P_\ell(t) - 1] f(t) dt - \int_{1-\varepsilon}^1 [P_\ell(t) - 1] f_k(t) dt \right]. \end{aligned} \quad (\text{A.16})$$

Using $0 \leq f_k \leq f$ and $|P_\ell(\mathbf{x} \cdot \mathbf{y})| \leq 1$ leads to

$$\begin{aligned} & \left| \int_{\mathbb{S}^2} f(\mathbf{x} \cdot \mathbf{z}) [P_\ell(\mathbf{y} \cdot \mathbf{z}) - P_\ell(\mathbf{x} \cdot \mathbf{y})] d\Omega(\mathbf{z}) - 2\pi P_\ell(\mathbf{x} \cdot \mathbf{y}) \gamma_\ell \right|, \\ & \leq 4\pi \left| \int_{1-\varepsilon}^1 [P_\ell(t) - 1] f(t) dt \right| + \left| \int_{C_\varepsilon(\mathbf{x})} f(\mathbf{x} \cdot \mathbf{z}) [P_\ell(\mathbf{y} \cdot \mathbf{z}) - P_\ell(\mathbf{x} \cdot \mathbf{y})] d\Omega(\mathbf{z}) \right|. \end{aligned} \quad (\text{A.17})$$

Both terms on the right-hand side of (A.17) go to zero as $\varepsilon \rightarrow 0$ or equivalently as $k \rightarrow \infty$. Finally, the space

$$\{\text{Lebesgue measurable } f : t \mapsto [P_\ell(t) - 1]f(t) \text{ absolutely integrable on } [-1, 1], \forall \ell = 0, 1, \dots\}, \quad (\text{A.18})$$

is the same as $t \mapsto (1 - t)f(t) \in L^1([-1, 1])$ since the only value of $t \in [-1, 1]$ for which $P_\ell(t) - 1 = 0$, $\forall \ell = 0, 1, \dots$, is $t = 1$. \square

B. Proof of $\mathcal{L}_\delta \rightarrow \mathcal{L}_0$ strongly as $\delta \rightarrow 0$

Let

$$u(\theta, \varphi) = \sum_{\ell=0}^{+\infty} \sum_{m=-\ell}^{+\ell} u_\ell^m Y_\ell^m(\theta, \varphi). \quad (\text{B.1})$$

Definition B.1 (see, e.g., [12]). For any $s \in \mathbb{R}$, the Sobolev space $H^s(\mathbb{S}^2)$ is the completion of $C^\infty(\mathbb{S}^2)$ with respect to the norm

$$\|u\|_{H^s(\mathbb{S}^2)}^2 = \sum_{\ell=0}^{+\infty} \sum_{m=-\ell}^{+\ell} \left(\ell + \frac{1}{2}\right)^{2s} |u_\ell^m|^2. \quad (\text{B.2})$$

Definition B.2. For every $\mathcal{L} : H^s(\mathbb{S}^2) \rightarrow H^{s-2}(\mathbb{S}^2)$, let $\|\cdot\|_s$ denote the induced operator norm defined by

$$\|\mathcal{L}\|_s = \sup_{0 \neq u \in H^s(\mathbb{S}^2)} \frac{\|\mathcal{L}u\|_{H^{s-2}(\mathbb{S}^2)}}{\|u\|_{H^s(\mathbb{S}^2)}}. \quad (\text{B.3})$$

Lemma B.3. For every $-1 < \alpha < 1$ and $0 < \delta \leq 2$,

$$-\ell(\ell + 1) \leq \lambda_\delta(\ell) \leq 0. \quad (\text{B.4})$$

Proof. The modulus of the spectrum of \mathcal{L}_δ is

$$\begin{aligned} |\lambda_\delta(\ell)| &= \left| \frac{(1+\alpha)2^{2-\alpha}}{\delta^2} \int_{-1}^1 \frac{P_\ell \left[1 - \frac{\delta^2}{2} \left(\frac{1-x}{2} \right) \right] - 1}{1-x} (1-x)^\alpha dx \right|, \\ &\leq \frac{(1+\alpha)2^{2-\alpha}}{\delta^2} \int_{-1}^1 \left| \frac{P_\ell \left[1 - \frac{\delta^2}{2} \left(\frac{1-x}{2} \right) \right] - 1}{1-x} \right| (1-x)^\alpha dx. \end{aligned} \quad (\text{B.5})$$

Using the inequalities

$$\begin{aligned} |P_\ell(x) - 1| &= |P_\ell(x) - P_{\ell-1}(x) + P_{\ell-1}(x) - 1| \leq |P_\ell(x) - P_{\ell-1}(x)| + |P_{\ell-1}(x) - 1|, \\ &\leq \sum_{\mu=1}^{\ell} |P_\mu(x) - P_{\mu-1}(x)|, \end{aligned} \quad (\text{B.6})$$

and the identity [33, §18.6.1 & 18.9.6]

$$P_\mu(x) - P_{\mu-1}(x) = -(1-x)P_{\mu-1}^{(1,0)}(x), \quad (\text{B.7})$$

where $P_{\mu-1}^{(1,0)}(x)$ is a Jacobi polynomial [33, §18.3], and since [33, §18.14.1]

$$\sup_{x \in [-1,1]} |P_{\mu-1}^{(1,0)}(x)| = \mu, \quad (\text{B.8})$$

we continue bounding the spectrum by

$$\begin{aligned} |\lambda_\delta(\ell)| &\leq \frac{(1+\alpha)2^{2-\alpha}}{\delta^2} \int_{-1}^1 \left\{ \sum_{\mu=1}^{\ell} \left| \frac{\delta^2}{2^2} P_{\mu-1}^{(1,0)} \left[1 - \frac{\delta^2}{2} \left(\frac{1-x}{2} \right) \right] \right| \right\} (1-x)^\alpha dx, \\ &= \frac{(1+\alpha)}{2^\alpha} \int_{-1}^1 \left\{ \sum_{\mu=1}^{\ell} \left| P_{\mu-1}^{(1,0)} \left[1 - \frac{\delta^2}{2} \left(\frac{1-x}{2} \right) \right] \right| \right\} (1-x)^\alpha dx, \\ &\leq \frac{(1+\alpha)}{2^\alpha} \int_{-1}^1 (1-x)^\alpha dx \sum_{\mu=1}^{\ell} \mu, \\ &= 2 \sum_{\mu=1}^{\ell} \mu = \ell(\ell + 1). \end{aligned} \quad (\text{B.9})$$

Since the integrand in (21) is non-positive, the spectrum is non-positive as well. \square

Theorem B.4. For every $-1 < \alpha < 1$, $0 < \delta \leq 2$, and $s \geq 0$, \mathcal{L}_δ is a bounded operator from $H^s(\mathbb{S}^2)$ to $H^{s-2}(\mathbb{S}^2)$, and

$$\|\mathcal{L}_\delta\|_s \leq \|\mathcal{L}_0\|_s < 1. \quad (\text{B.10})$$

Proof. These inequalities follow naturally from the definition of the induced operator norm, Lemma B.3, and the completeness of spherical harmonics in $H^s(\mathbb{S}^2) \leftrightarrow L^2(\mathbb{S}^2)$. \square

Lemma B.5. For every $\ell = 0, 1, \dots$, $-1 < \alpha < 1$ and $\varepsilon > 0$, there exists $0 < \delta \leq \frac{4\sqrt{\varepsilon}}{\ell+2}$ such that

$$|\lambda_\delta(\ell) - \lambda_0(\ell)| \leq \varepsilon |\lambda_0(\ell)|. \quad (\text{B.11})$$

Proof. By the Lagrange form of the remainder in Taylor's theorem, there exists a $\xi \in [-1, 1]$ such that

$$P_\ell \left[1 - \frac{\delta^2}{2} \left(\frac{1-x}{2} \right) \right] = P_\ell(1) - P'_\ell(1) \frac{\delta^2}{2^2} (1-x) + P''_\ell \left[1 - \frac{\delta^2}{2} \left(\frac{1-\xi}{2} \right) \right] \frac{\delta^4}{2^4} \frac{(1-x)^2}{2}. \quad (\text{B.12})$$

Rearranging terms,

$$\frac{P_\ell \left[1 - \frac{\delta^2}{2} \left(\frac{1-x}{2} \right) \right] - 1}{1-x} = -\frac{\delta^2}{2^2} \frac{\ell(\ell+1)}{2} + P''_\ell \left[1 - \frac{\delta^2}{2} \left(\frac{1-\xi}{2} \right) \right] \frac{\delta^4}{2^4} \frac{(1-x)}{2}. \quad (\text{B.13})$$

Now, the second derivative of the Legendre polynomials is given in terms of the Jacobi polynomials [33, §18.3]

$$P''_\ell(x) = \frac{(\ell+1)(\ell+2)}{2^2} P_{\ell-2}^{(2,2)}(x), \quad (\text{B.14})$$

and since [33, §18.14.1]

$$\sup_{x \in [-1,1]} |P_{\ell-2}^{(2,2)}(x)| = \frac{(\ell-1)\ell}{2}, \quad (\text{B.15})$$

we obtain

$$\begin{aligned} |\lambda_\delta(\ell) - \lambda_0(\ell)| &\leq \frac{(\alpha+1)}{2^\alpha} \int_{-1}^1 \frac{(\ell-1)\ell(\ell+1)(\ell+2)\delta^2}{2^6} (1-x)^{\alpha+1} dx, \\ &\leq \frac{\alpha+1}{\alpha+2} \frac{(\ell-1)\ell(\ell+1)(\ell+2)\delta^2}{2^4}, \\ &\leq \frac{(\ell-1)\ell(\ell+1)(\ell+2)\delta^2}{2^4}, \\ &\leq \frac{\ell(\ell+1)(\ell+2)^2\delta^2}{2^4} = \varepsilon |\lambda_0(\ell)|. \end{aligned} \quad (\text{B.16})$$

□

We are now in a position to prove strong convergence of the nonlocal operators to the Laplace–Beltrami operator.

Theorem B.6. For every $-1 < \alpha < 1$ and $s \geq 0$, $\mathcal{L}_\delta \rightarrow \mathcal{L}_0$ strongly as $\delta \rightarrow 0$. That is,

$$\forall u \in H^s(\mathbb{S}^2), \quad \|(\mathcal{L}_\delta - \mathcal{L}_0)u\|_{H^{s-2}(\mathbb{S}^2)} \rightarrow 0, \quad \text{as } \delta \rightarrow 0. \quad (\text{B.17})$$

Proof. Let

$$u_n(\theta, \varphi) = \sum_{\ell=0}^{+n} \sum_{m=-\ell}^{+\ell} u_\ell^m Y_\ell^m(\theta, \varphi), \quad (\text{B.18})$$

be the degree- n truncation of $u \in H^s(\mathbb{S}^2)$. For every $\varepsilon > 0$ and $n = 0, 1, \dots$, there exists $0 < \delta \leq \frac{4\sqrt{\varepsilon}}{n+2}$ such that

$$\begin{aligned} \|(\mathcal{L}_\delta - \mathcal{L}_0)u\|_{H^{s-2}(\mathbb{S}^2)} &\leq \|(\mathcal{L}_\delta - \mathcal{L}_0)u_n\|_{H^{s-2}(\mathbb{S}^2)} + \|\mathcal{L}_\delta(u - u_n)\|_{H^{s-2}(\mathbb{S}^2)} + \|\mathcal{L}_0(u - u_n)\|_{H^{s-2}(\mathbb{S}^2)}, \\ &\leq \|(\mathcal{L}_\delta - \mathcal{L}_0)u_n\|_{H^{s-2}(\mathbb{S}^2)} + (\|\mathcal{L}_\delta\|_s + \|\mathcal{L}_0\|_s) \|u - u_n\|_{H^s(\mathbb{S}^2)}, \\ &< \varepsilon \|u\|_{H^s(\mathbb{S}^2)} + 2 \|u - u_n\|_{H^s(\mathbb{S}^2)}. \end{aligned} \quad (\text{B.19})$$

Thus, the norm is bounded by the first term that is arbitrarily small and the second term that converges to 0 as $n \rightarrow \infty$ or equivalently as $\delta \rightarrow 0$; for definiteness, choose

$$\varepsilon = \frac{1}{(n+2)^2}, \quad \delta = \frac{4}{(n+2)^2}, \quad \text{and take } n \rightarrow \infty. \quad (\text{B.20})$$

Convergence of the second term follows from the completeness of spherical harmonics in $H^s(\mathbb{S}^2) \hookrightarrow L^2(\mathbb{S}^2)$. □